POLITECNICO DI TORINO
Repository ISTITUZIONALE

A Novel Framework for Parametric Loewner Matrix Interpolation

Terms of use:

Publisher copyright

(Article begins on next page)

20 April 2024

A Novel Framework for Parametric Loewner Matrix Interpolation

Yi Qing Xiao, Stefano Grivet-Talocia, *Fellow, IEEE,* Paolo Manfredi, *Senior Member, IEEE,* Roni Khazaka, *Senior Member, IEEE.*

Abstract—The generation of black-box macromodels of passive components at the chip, package and board levels has become an important step of the electronic design automation work-flow. The Vector Fitting scheme is a very popular method for the extraction of such macromodels, and several multivariate extensions are now available for embedding external parameters in the model structure, thus enabling model-based variability analysis and design optimization. The Loewner matrix inter-polation framework was recently suggested as an effective and promising alternative macromodeling approach to Vector Fitting. In this paper, we propose a parametric version of Loewner in-terpolation which embeds orthogonal polynomials as an integral part of the parameterization framework. This approach is shown to be efficient and accurate, and presents various advantages with respect to competing multivariate rational interpolation methods. These advantages include a better control of model smoothness in the parameter space, and a particularly efficient implementation of the singular value decomposition, which is the core of the model extraction scheme. These advantages are confirmed through several examples relevant for signal and power integrity applications.

Index Terms—Loewner matrix, macromodeling, model order reduction, parameterized modeling, orthogonal polynomial basis, rational approximation, singular value decomposition (SVD), system identification.

I. INTRODUCTION

Signal and power integrity have recently become one of the key design bottlenecks for high-speed systems. As a result, it is now critical to include accurate broadband models of pack-ages, interconnects, connectors, and other passive elements as part of the electronic design automation work-flow. Further-more, it is also important for such models to be parametric with respect to key geometric and material parameters in order to enable standard EDA methodologies such as optimization, design centering, and design space exploration. While it is possible to obtain the frequency-domain characteristics of such passive components using measurement or full-wave simulation, it is usually not possible to construct accurate time-domain models that are compatible with SPICE-class circuit simulators by using theoretical physics-based methods. As a result, a considerable effort has been made in the area of numerical black-box macromodeling, including parameterized macromodeling, where a time-domain macromodel is numeri-cally constructed based on frequency-domain S-parameter data

Y. Q. Xiao and R. Khazaka are with the Dept. of Electrical and Com-puter Engineering, McGill University, Montréal QC H3A 0E9, Canada (yi.q.xiao@mail.mcgill.ca; roni.khazaka@mcgill.ca).

S. Grivet-Talocia and P. Manfredi are with the Dept. of Electron-ics and Telecommunications, Politecnico di Torino, Turin 10129, Italy ({stefano.grivet; paolo.manfredi}@polito.it).

obtained from either measurement or simulation. For a detailed overview on theory and applications, see [1].

While a number of possible approaches have been pro-posed for black-box time-domain macromodeling of passive structures [2]–[10], methods based on Vector Fitting (VF) [8] have emerged as the common approach used in commercial tools. As a result, a considerable amount of research has been devoted to developing parametric VF-based models [11]–[22]. The overall goal of these methods is to produce a macromodel that is a function of the desired design parameter(s), while at the same time addressing issues of accuracy, robustness, stability and passivity. In [11], [14], efficient methods were proposed based on the interpolation of root univariate macro-models. These methods have the inherent merit of producing guaranteed stable and passive parameterizations. However, they assume fixed-pole systems, limiting applicability depend-ing on the problem being considered. This problem was atten-uated in [12], which allowed for parameterized poles through local frequency transformations. The methods in [13], [19], [20], [22] also allow for parameter dependent poles. However, they require the solution of computationally expensive linear matrix inequalities. In general, all above methods assume a model structure that is derived from some interpolation applied to non-parameterized models, which in turn are available from standard VF. The accuracy of the respective parameterizations depends on the number of these root non-parameterized mod-els, which may grow very large in case of a high-dimensional parameter space and large variability. This problem is partly mitigated by methods based on the Parameterized Sanathanan-Koerner (PSK) iteration [17], [18], [21], [23], [24]. These methods are unable to enforce model passivity by construction, but robust and efficient postprocessing methods exist for this purpose [25], [26].

Recently, a promising framework based on Loewner Ma-trix (LM) interpolation has been proposed as an alterna-tive to VF for broadband time-domain macromodeling [27]–[40]. The main advantage of the LM approach is a strong system-theoretical framework, which supports numerical im-plementation with a guarantee of important properties such as exact frequency-domain interpolation and optimal model order. In [41], a parametric method in the Loewner frame-work was proposed where principal component analysis was used to obtain continuous macromodels that are suitable for interpolation. However, this approach is only suitable for systems where the order is relatively constant with respect to the parameters [42]. A more direct method for obtaining Loewner-based parametric macromodels leverages multivari-

ate LM methods [43], [44], which extend the concept of LM interpolation to the multivariate case, one variable being the frequency, and the others being the desired circuit parameters. Two main issues affect this approach: first, the size of the LM increases at an exponential rate due to the concurrent presence of all data samples in the main matrix formulation; second, the model parameterization may induce non-smooth approximations due to strict interpolation conditions that are enforced in the parametric data set. This problem will be illustrated and discussed later through numerical examples, in Section IV.

In this paper, we propose a new model structure and related identification method for parametric macromodeling in the bluebarycentric form of the LM framework. In contrast to using higher LM dimensions as in [43], [44], we enrich a standard univariate LM-based rational function interpolation by embedding a parameter dependence in the coefficients through a polynomial expansion. The proposed method has a number of advantages. First, the transfer function is obtained directly using a Singular Value Decomposition (SVD) on the parametric LM, without the need for iterations (as required by VF and PSK schemes instead). Second, the proposed approach does not require the repeated generation of univariate root macromodels along various grid points in the parameter space, since a parameterized model is obtained in a single pass. Third, unlike the standard Loewner-based methods [43], the exact interpolation conditions at the available data points are relaxed by a least-squares-based polynomial approximation. This reduces the likelihood of over-fitting and non-smooth inter-sample behavior. Finally, the proposed structure of the LM allows us to very efficiently compute the SVD of the LM matrix, which is the most computationally expensive part of the Loewner approach. These advantages are illustrated on several test cases.

II. PRELIMINARIES AND NOTATION

A. Background: Standard Loewner Interpolation

The objective of the standard Loewner method is to interpolate a set of given frequency response samples

$$\mathcal{H} = \{H(s_l); \ s_l \in \mathcal{S}\}, \tag{1}$$

where $H(s_l) \in \mathbb{C}$ is the (scalar) transfer function of the underlying system evaluated at s_l and

$$\mathcal{S} = \{s_l\}_{l=1}^{\bar{l}} \tag{2}$$

is a set of complex frequency samples with no repeated entries; usually, $s_l = \jmath\omega_l$ with $\omega_l \in [\omega_{\min}, \omega_{\max}]$ being the frequency band of interest.

The set $\mathcal{S}$ is partitioned as $\mathcal{S} = \Lambda \cup \mathcal{M}$, where

$$\Lambda = \{\lambda_1, \cdots, \lambda_{\bar{j}}\}, \quad \mathcal{M} = \{\mu_1, \cdots, \mu_{\bar{\imath}}\} \tag{3}$$

with corresponding data set partitions:

$$\mathcal{H}_\Lambda = \{H(\lambda_j); \ \lambda_j \in \Lambda\}, \quad \mathcal{H}_\mathcal{M} = \{H(\mu_i); \ \mu_i \in \mathcal{M}\}. \tag{4}$$

The Loewner method is based on the following rational approximation in barycentric form

$$H(s) \approx \widetilde{H}(s) = \frac{\displaystyle\sum_{j=1}^{\bar{j}} \frac{c_j H(\lambda_j)}{s - \lambda_j}}{\displaystyle\sum_{j=1}^{\bar{j}} \frac{c_j}{s - \lambda_j}}. \tag{5}$$

Given a non-trivial choice of coefficients $\{c_j\}_{j=1}^{\bar{j}}$, the rational model $\widetilde{H}(s)$ in (5) interpolates $\mathcal{H}_\Lambda$ exactly by construction. The guiding condition in determining a suitable set $\{c_j\}_{j=1}^{\bar{j}}$ is the minimization of the approximation error of data points in $\mathcal{H}_\mathcal{M}$. Setting the error $H(\mu_i) - \widetilde{H}(\mu_i) \approx 0$ for all i's leads to the condition

$$\sum_{j=1}^{\bar{j}} \frac{c_j (H(\mu_i) - H(\lambda_j))}{\mu_i - \lambda_j} \approx 0, \quad i = 1, \ldots, \bar{\imath} \tag{6}$$

which is written in compact matrix form as

$$\mathbb{L}\, \boldsymbol{c} \approx \boldsymbol{0}_{\bar{\imath} \times 1} \tag{7}$$

where vector $\boldsymbol{c}$ collects all coefficients c_j and

$$\mathbb{L} = \begin{bmatrix} \frac{H(\mu_1)-H(\lambda_1)}{\mu_1-\lambda_1} & \frac{H(\mu_1)-H(\lambda_2)}{\mu_1-\lambda_2} & \cdots & \frac{H(\mu_1)-H(\lambda_{\bar{j}})}{\mu_1-\lambda_{\bar{j}}} \\ \frac{H(\mu_2)-H(\lambda_1)}{\mu_2-\lambda_1} & \frac{H(\mu_2)-H(\lambda_2)}{\mu_2-\lambda_2} & \cdots & \frac{H(\mu_2)-H(\lambda_{\bar{j}})}{\mu_2-\lambda_{\bar{j}}} \\ \vdots & \vdots & \ddots & \vdots \\ \frac{H(\mu_{\bar{\imath}})-H(\lambda_1)}{\mu_{\bar{\imath}}-\lambda_1} & \frac{H(\mu_{\bar{\imath}})-H(\lambda_2)}{\mu_{\bar{\imath}}-\lambda_2} & \cdots & \frac{H(\mu_{\bar{\imath}})-H(\lambda_{\bar{j}})}{\mu_{\bar{\imath}}-\lambda_{\bar{j}}} \end{bmatrix} \tag{8}$$

is the so-called LM based on the adopted data partition. The right singular vector associated to one of the smallest singular values $\sigma_\star < \epsilon$ of $\mathbb{L}$, where ϵ is a predetermined threshold, can be chosen as a solution for (7). We remark that the above derivation can be easily extended to the Multi-Input Multi-Output (MIMO) case. We provide such details while presenting the proposed parameterized macromodeling method in the following sections.

The barycentric model (5) is easily converted to an equivalent pole-reside form or realized as a state-space system. The latter is also readily synthesized in an equivalent lumped circuit, e.g., for circuit-oriented system-level simulation. See [1] for details.

B. Problem Statement

Assume an underlying system with $\bar{m}$ inputs and $\bar{p}$ outputs, with an unknown frequency response $\boldsymbol{H}(s, \theta)$ that depends on both frequency s and some external parameter θ, which in the following we assume to be a scalar variable defined in a finite range $[\theta_{\min}, \theta_{\max}]$. The system is known through a set of measurements

$$\mathcal{H} = \{\boldsymbol{H}(s_l, \theta_q); \ s_l \in \mathcal{S}, \ \theta_q \in \Theta\} \tag{9}$$

where

- $\boldsymbol{H}(s_l, \theta_q) \in \mathbb{C}^{\bar{p} \times \bar{m}}$ is the transfer function of the system evaluated at s_l and θ_q;
- $\Theta = \{\theta_q\}_{q=1}^{\bar{q}}$ is a set of single parameter samples with no repeated entries spanning the parameter

range $[\theta_{\min}, \theta_{\max}]$, with corresponding index set $\mathcal{Q} = \{1, \cdots, \bar{q}\}$;

and where $\mathcal{S}$ and s_l are defined as in (2). The goal is to compute a parameterized model whose frequency response approximates the data set (9) accurately.

C. Fitting Conditions

Following the standard LM procedure of Section II-A, we partition the data set $\mathcal{H}$ by dividing the frequency samples $\mathcal{S}$ into two mutually exclusive partitions

$$\Lambda = \{\lambda_1, \cdots, \lambda_{\bar{j}}\}, \quad \mathcal{M} = \{\mu_1, \cdots, \mu_{\bar{\imath}}\} \quad (10)$$

with $\Lambda \cup \mathcal{M} = \mathcal{S}$, $\Lambda \cap \mathcal{M} = \emptyset$, and with corresponding index sets $\mathcal{J} = \{1, \ldots, \bar{j}\}$, $\mathcal{I} = \{1, \ldots, \bar{\imath}\}$, obtaining

$$\begin{aligned} \mathcal{H}_\Lambda &= \{\boldsymbol{H}(\lambda_j, \theta_q); \ \lambda_j \in \Lambda, \ \theta_q \in \Theta\}, \\ \mathcal{H}_\mathcal{M} &= \{\boldsymbol{H}(\mu_i, \theta_q); \ \mu_i \in \mathcal{M}, \ \theta_q \in \Theta\}. \end{aligned} \quad (11)$$

Note that, differently from [43], we only perform a partition of the frequency samples, whereas all parameter samples are considered as a single set. The frequency points in partition Λ are chosen to be linearly spaced along the bandwidth of interest. The number of points in Λ determines the order of the system, and it is chosen according to the greedy method described in Section III-H.

We want to approximate the data set $\mathcal{H}$ by extending the standard Loewner framework to the parametric case. To this end, we define the following parameterized barycentric rational function form

$$\boldsymbol{H}(s, \theta) \approx \widetilde{\boldsymbol{H}}(s, \theta) = \frac{\displaystyle\sum_{j=1}^{\bar{j}} \frac{c_j(\theta) \boldsymbol{H}(\lambda_j, \theta)}{s - \lambda_j}}{\displaystyle\sum_{j=1}^{\bar{j}} \frac{c_j(\theta)}{s - \lambda_j}}, \quad \forall \theta. \quad (12)$$

It can be easily shown that, by construction, no matter the choice of non-trivial functions $\{c_j(\theta)\}_{j=1}^{\bar{j}}$, the model $\widetilde{\boldsymbol{H}}(s, \theta)$ in (12) provides an exact interpolation at all points in the first frequency partition Λ, and uniformly in the parameter space, as

$$\widetilde{\boldsymbol{H}}(\lambda_j, \theta) \equiv \boldsymbol{H}(\lambda_j, \theta), \quad \forall \lambda_j \in \Lambda, \forall \theta. \quad (13)$$

The determination of an appropriate set of functions $\{c_j(\theta)\}_{j=1}^{\bar{j}}$ in (12) will be guided by additional interpolation conditions, to be enforced at the second frequency partition points $\mathcal{M}$ and at the available discrete parameter points Θ through

$$\boldsymbol{H}(s_l, \theta_q) \equiv \widetilde{\boldsymbol{H}}(s_l, \theta_q), \quad \forall s_l \in \mathcal{S}, \forall \theta_q \in \Theta \quad (14)$$

D. Polynomial Basis

A key part of the proposed algorithm consists of using a polynomial basis to characterize and approximate the transfer function dependence on the parameter variable θ. We define a polynomial basis as $\{\varphi_k(\theta)\}_{k=1}^{\bar{k}}$, where $\varphi_k(\theta)$ is a polynomial of degree $k - 1$. For now, no further assumptions are made on the polynomials such as orthogonality and type of polynomials, except linear independence of the basis elements. In particular, any polynomial basis with bounded support in the parameter space can be used for this purpose, e.g., Legendre or Chebyshev polynomials. To avoid any confusion, we remark that the specific choice of parameter basis functions has no relation with the derivation of the barycentric representation in (5), which is well-known to be a reformulation of the Lagrange polynomial interpolation formula.

III. FORMULATION

This section describes the proposed multivariate LM interpolation scheme. We first describe how the parametric dependence of the transfer function is captured using a polynomial expansion. Then, the fitting conditions for frequency partitions Λ and $\mathcal{M}$ are described and used to derive an appropriate generalization of the LM, suitable for the parametric case at hand.

A. Parametric Dependence

The scalar case $\bar{m} = \bar{p} = 1$ is discussed first, followed by a generalization to the MIMO case. Throughout Sections III-A to III-C, we denote the underlying scalar system transfer function with $H(s, \theta)$ and the corresponding model (12) as $\widetilde{H}(s, \theta)$.

Since (12) depends on the continuous variable θ, it cannot be enforced exactly $\forall \theta \in [\theta_{\min}, \theta_{\max}]$. Therefore, we perform an approximation by expanding the unknown functions $\{c_j(\theta)\}_{j=1}^{\bar{j}}$ using the polynomial basis $\{\varphi_k(\theta)\}_{k=1}^{\bar{k}}$ as

$$c_j(\theta) \approx \sum_{k=1}^{\bar{k}} c_{jk} \varphi_k(\theta). \quad (15)$$

The coefficients c_{jk}, collected in a matrix $\boldsymbol{C} \in \mathbb{C}^{\bar{j} \times \bar{k}}$, will be our main unknowns in the following. We apply a similar approximation, using a different set of unknown coefficients d_{jk} collected in a matrix $\boldsymbol{D} \in \mathbb{C}^{\bar{j} \times \bar{k}}$, to the numerator of (12):

$$c_j(\theta) H(\lambda_j, \theta) \approx \sum_{k=1}^{\bar{k}} d_{jk} \varphi_k(\theta). \quad (16)$$

Combining the expansions (15) and (16) with (12) leads to the model structure

$$\widetilde{H}(s, \theta) \approx \widehat{H}(s, \theta) = \frac{\displaystyle\sum_{j=1}^{\bar{j}} \frac{\sum_{k=1}^{\bar{k}} d_{jk} \varphi_k(\theta)}{s - \lambda_j}}{\displaystyle\sum_{j=1}^{\bar{j}} \frac{\sum_{k=1}^{\bar{k}} c_{jk} \varphi_k(\theta)}{s - \lambda_j}}, \quad (17)$$

which can be interpreted as an approximation to the exact condition (12) based on the adopted polynomial approximation. For later convenience, we denote the columns of $\boldsymbol{C}^T$ and $\boldsymbol{D}^T$, respectively, as $\boldsymbol{c}_j$ and $\boldsymbol{d}_j$, for any $j \in \mathcal{J}$.

B. Interpolating Data in the First Partition

Our objective in this section is to define the conditions that the coefficients c_{jk} and d_{jk} must satisfy so that the model (17) interpolates all data in $\mathcal{H}_\Lambda$. This is obtained by enforcing

$$\widehat{H}(\lambda_j, \theta_q) \equiv H(\lambda_j, \theta_q), \quad \forall j \in \mathcal{J}, \forall q \in \mathcal{Q} \quad (18)$$

According to property (13), if the following conditions hold

$$\sum_{k=1}^{\bar{k}} d_{jk}\varphi_k(\theta_q) \equiv c_j(\theta_q)H(\lambda_j,\theta_q) \qquad (19)$$

$$\sum_{k=1}^{\bar{k}} c_{jk}\varphi_k(\theta_q) \equiv c_j(\theta_q) \qquad (20)$$

for $\forall j \in \mathcal{J}$ and $\forall q \in \mathcal{Q}$, then (18) is naturally achieved. Combining (20) and (19) leads to

$$\sum_{k=1}^{\bar{k}} d_{jk}\varphi_k(\theta_q) = \sum_{k=1}^{\bar{k}} c_{jk}\varphi_k(\theta_q)H(\lambda_j,\theta_q) \qquad (21)$$

which can be written in a compact form as

$$\boldsymbol{\varphi}_q^T \boldsymbol{d}_j = H(\lambda_j,\theta_q)\,\boldsymbol{\varphi}_q^T \boldsymbol{c}_j. \qquad (22)$$

where

$$\boldsymbol{\varphi}_q^T = \begin{bmatrix} \varphi_1(\theta_q) & \varphi_2(\theta_q) & \dots & \varphi_{\bar{k}}(\theta_q) \end{bmatrix} \in \mathbb{R}^{1\times\bar{k}} \qquad (23)$$

Defining now matrix $\boldsymbol{\Phi} \in \mathbb{R}^{\bar{q}\times\bar{k}}$ with elements $\Phi_{qk} = \varphi_k(\theta_q)$, and collecting $H(\lambda_j,\theta_q)$ for all $\theta_q \in \Theta$ at each $j \in \mathcal{J}$ into

$$\boldsymbol{W}_j = \mathrm{diag}\{H(\lambda_j,\theta_q)\}_{q=1}^{\bar{q}}, \qquad (24)$$

we can write (22) for all q's as

$$\boldsymbol{\Phi}\boldsymbol{d}_j = \boldsymbol{W}_j\boldsymbol{\Phi}\boldsymbol{c}_j. \qquad (25)$$

The exact solvability of (25) for $\boldsymbol{d}_j$ depends on the size of the matrix $\boldsymbol{\Phi}$, which in turns depends on the cardinality of the polynomial basis $\bar{k}$ and on the number of available parameter grid points $\bar{q}$. Leaving out of our discussion the unimportant case $\bar{k} > \bar{q}$, corresponding to insufficient grid points (or, equivalently, excessive polynomial order), we have two possibilities:

$\bar{k} = \bar{q}$: the number of polynomial basis functions matches the number of parameter grid points. Exact interpolation is possible, and coherently matrix $\boldsymbol{\Phi}$ is square.

$\bar{k} < \bar{q}$: there are more parameter grid points than polynomial basis functions, so that exact interpolation cannot be enforced, and only a least-squares type of fitting is possible.

Both cases can be collectively written as

$$\boldsymbol{d}_j = \boldsymbol{\Phi}^\dagger \boldsymbol{W}_j\boldsymbol{\Phi}\boldsymbol{c}_j, \quad \forall j \in \mathcal{J} \qquad (26)$$

where $\boldsymbol{\Phi}^\dagger$ is the Moore-Penrose pseudoinverse of $\boldsymbol{\Phi}$. If $\bar{k} = \bar{q}$, this pseudo-inverse coincides with the actual inverse (which exists thanks to the linear independence of the adopted polynomial basis) and exact interpolation holds.

C. Interpolating Data in the Second Partition

At this point, we know that, by maintaining the relation (21) through enforcing (25), we can make sure that $\widehat{H}(s,\theta)$, as defined in (17), interpolates or approximates the data in the first partition $\mathcal{H}_\Lambda$. In this sub-section, we define the conditions for determining the denominator coefficients c_{jk} such that the model $\widehat{H}(s,\theta)$ approximates also the data in the second partition $\mathcal{H}_\mathcal{M}$.

We start by evaluating the model $\widehat{H}(s,\theta)$ at points in $\mathcal{M}$:

$$H(\mu_i,\theta_q) \approx \widehat{H}(\mu_i,\theta_q) = \frac{\displaystyle\sum_{j=1}^{\bar{j}}\frac{\sum_{k=1}^{\bar{k}} d_{jk}\varphi_k(\theta_q)}{\mu_i - \lambda_j}}{\displaystyle\sum_{j=1}^{\bar{j}}\frac{\sum_{k=1}^{\bar{k}} c_{jk}\varphi_k(\theta_q)}{\mu_i - \lambda_j}} \qquad (27)$$

Multiplying by the denominator leads to

$$H(\mu_i,\theta_q)\sum_{j=1}^{\bar{j}}\frac{\sum_{k=1}^{\bar{k}} c_{jk}\varphi_k(\theta_q)}{\mu_i - \lambda_j} \approx \sum_{j=1}^{\bar{j}}\frac{\sum_{k=1}^{\bar{k}} d_{jk}\varphi_k(\theta_q)}{\mu_i - \lambda_j} \qquad (28)$$

which is rewritten by collecting all terms into a single sum as

$$\sum_{j=1}^{\bar{j}}\frac{\sum_{k=1}^{\bar{k}}[c_{jk}H(\mu_i,\theta_q) - d_{jk}]\varphi_k(\theta_q)}{\mu_i - \lambda_j} \approx 0, \qquad (29)$$

which needs to be enforced $\forall i \in \mathcal{I}$ and $\forall q \in \mathcal{Q}$. Defining now

$$\boldsymbol{V}_i = \mathrm{diag}\{H(\mu_i,\theta_q)\}_{q=1}^{\bar{q}}, \qquad (30)$$

and enforcing (29) for all $q \in \mathcal{Q}$, leads to the compact form

$$\sum_{j=1}^{\bar{j}}\frac{1}{\mu_i - \lambda_j}\left[\boldsymbol{V}_i - \boldsymbol{\Phi}\boldsymbol{\Phi}^\dagger\boldsymbol{W}_j\right]\boldsymbol{\Phi}\boldsymbol{c}_j \approx \boldsymbol{0}_{\bar{q}\times 1}, \qquad (31)$$

where the relationship (26) between the numerator and denominator coefficients has been used. We can thus define the following extended Loewner matrix in this scalar case as

$$\mathbb{L} = \begin{bmatrix} \mathbb{L}_{11} & \mathbb{L}_{12} & \dots & \mathbb{L}_{1\bar{j}} \\ \mathbb{L}_{21} & \mathbb{L}_{22} & \dots & \mathbb{L}_{2\bar{j}} \\ \vdots & \vdots & \ddots & \vdots \\ \mathbb{L}_{\bar{i}1} & \mathbb{L}_{\bar{i}2} & \dots & \mathbb{L}_{\bar{i}\bar{j}} \end{bmatrix} \in \mathbb{C}^{\bar{i}\bar{q}\times\bar{j}\bar{k}} \qquad (32)$$

with individual blocks

$$\mathbb{L}_{ij} = \frac{1}{\mu_i - \lambda_j}\left[\boldsymbol{V}_i - \boldsymbol{\Phi}\boldsymbol{\Phi}^\dagger\boldsymbol{W}_j\right]\boldsymbol{\Phi} \in \mathbb{C}^{\bar{q}\times\bar{k}}. \qquad (33)$$

Casting (31) for all $i \in \mathcal{I}$ leads to the compact matrix form

$$\mathbb{L}\boldsymbol{c} \approx \boldsymbol{0}_{\bar{i}\bar{q}\times 1}. \qquad (34)$$

where the unknown coefficients are collected into a single vector $\boldsymbol{c} = \mathrm{vec}\{\boldsymbol{C}^T\}$.

D. Enforcing Realness

The frequency response of physically-consistent (parameterized) models should satisfy the appropriate realness condition $\widehat{H}(s^*,\theta) = \widehat{H}^*(s,\theta)$, where * denotes the complex conjugate, in order to guarantee a real-valued impulse response. The proposed method is easily modified by enforcing such condition using the following standard procedure.

Assuming that $s = 0 \notin \mathcal{S}$ (i.e., it belongs neither to first nor to second partition data), we recast the model (17) as

$$\widehat{H}(s,\theta) = \frac{\displaystyle\sum_{j=1}^{\bar{j}}\left[\frac{\sum_{k=1}^{\bar{k}} d_{jk}\varphi_k(\theta)}{s - \lambda_j} + \frac{\sum_{k=1}^{\bar{k}} d_{jk}^*\varphi_k(\theta)}{s - \lambda_j^*}\right]}{\displaystyle\sum_{j=1}^{\bar{j}}\left[\frac{\sum_{k=1}^{\bar{k}} c_{jk}\varphi_k(\theta)}{s - \lambda_j} + \frac{\sum_{k=1}^{\bar{k}} c_{jk}^*\varphi_k(\theta)}{s - \lambda_j^*}\right]}. \qquad (35)$$

This is equivalent to including in the first partition also the data samples at negative (conjugate) frequencies. Realness is guaranteed by assigning complex conjugate coefficients c_{jk}^*, d_{jk}^* in correspondence to the conjugate frequency points λ_j^*.

Repeating the above derivations and defining

$$
\begin{aligned}
\mathbb{A}_{ij} &= \frac{1}{\mu_i - \lambda_j} \left[\boldsymbol{V}_i - \boldsymbol{\Phi}\boldsymbol{\Phi}^\dagger \boldsymbol{W}_j \right] \boldsymbol{\Phi} = \mathbb{A}_{ij}' + \jmath\, \mathbb{A}_{ij}'' \\
\mathbb{B}_{ij} &= \frac{1}{\mu_i - \lambda_j^*} \left[\boldsymbol{V}_i - \boldsymbol{\Phi}\boldsymbol{\Phi}^\dagger \boldsymbol{W}_j^* \right] \boldsymbol{\Phi} = \mathbb{B}_{ij}' + \jmath\, \mathbb{B}_{ij}''
\end{aligned}
\tag{36}
$$

where $'$ and $''$ denote real and imaginary parts, respectively, as well as

$$
\widehat{\mathbb{L}}_{ij} = \begin{bmatrix} \mathbb{A}_{ij}' + \mathbb{B}_{ij}' & \mathbb{B}_{ij}'' - \mathbb{A}_{ij}'' \\ \mathbb{A}_{ij}'' + \mathbb{B}_{ij}'' & \mathbb{A}_{ij}' - \mathbb{B}_{ij}' \end{bmatrix} \in \mathbb{R}^{2\bar{q} \times 2\bar{k}}
\tag{37}
$$

we see that (34) is rewritten as

$$
\widehat{\mathbb{L}}\, \widehat{\boldsymbol{c}} \approx \boldsymbol{0}_{2\bar{\imath}\bar{q} \times 1}.
\tag{38}
$$

where $\widehat{\mathbb{L}}$ collects the blocks $\widehat{\mathbb{L}}_{ij}$ as in (32), and

$$
\widehat{\boldsymbol{c}} = \begin{pmatrix} \widehat{\boldsymbol{c}}_1^T & \cdots & \widehat{\boldsymbol{c}}_{\bar{\jmath}}^T \end{pmatrix}^T \in \mathbb{R}^{2\bar{\jmath}\bar{k}}, \quad \text{with} \quad \widehat{\boldsymbol{c}}_j = \begin{pmatrix} \boldsymbol{c}_j' \\ \boldsymbol{c}_j'' \end{pmatrix}
\tag{39}
$$

collects the real and imaginary parts of all model coefficients. We remark that, in this real-valued formulation, increasing the first partition by one point $\bar{\jmath} \leftarrow \bar{\jmath} + 1$ will lead to a number of macromodel poles that is increased by two.

E. The MIMO Case

Let us consider now the MIMO case with $\bar{m}$ inputs and $\bar{p}$ outputs, so that $\boldsymbol{H}(s, \theta) \in \mathbb{C}^{\bar{p} \times \bar{m}}$. The proposed model structure, after polynomial expansion (17), generalizes to

$$
\widehat{\boldsymbol{H}}(s, \theta) = \frac{\displaystyle\sum_{j=1}^{\bar{\jmath}} \frac{\sum_{k=1}^{\bar{k}} \boldsymbol{D}_{jk}\varphi_k(\theta)}{s - \lambda_j}}{\displaystyle\sum_{j=1}^{\bar{\jmath}} \frac{\sum_{k=1}^{\bar{k}} c_{jk}\varphi_k(\theta)}{s - \lambda_j}},
\tag{40}
$$

from which we observe that the denominator remains unchanged, still being fully characterized by the set of scalar coefficients c_{jk}. This induces a parameterization of model poles (the zeros of the denominator) which will be common to all transfer matrix elements of the model. What differentiates the various model responses are the numerator coefficients $\boldsymbol{D}_{jk}$, which are now $\bar{p} \times \bar{m}$ matrices.

We repeat all derivations of Sections III-B to III-C, but applied to a single element (p, m) of the MIMO transfer function $H_{pm}(s, \theta)$, with $1 \le m \le \bar{m}$ and $1 \le p \le \bar{p}$. The only difference with respect to the scalar case is that the data matrices $\boldsymbol{W}_j$, $\boldsymbol{V}_i$ in (24) and (30) should now be indexed by (p, m):

$$
\boldsymbol{W}_j^{p,m} = \operatorname{diag}\{H_{pm}(\lambda_j, \theta_q)\}_{q=1}^{\bar{q}},
\tag{41}
$$

$$
\boldsymbol{V}_i^{p,m} = \operatorname{diag}\{H_{pm}(\mu_i, \theta_q)\}_{q=1}^{\bar{q}},
\tag{42}
$$

as well as the numerator coefficients $\boldsymbol{d}_j \to \boldsymbol{d}_j^{p,m}$, which collect in column vectors all matrix elements $D_{jk}^{p,m}$ for each

fixed (p, m) and j, with $k = 1, \ldots, \bar{k}$. Correspondingly, we generalize (26) for each (p, m) to

$$
\boldsymbol{d}_j^{p,m} = \boldsymbol{\Phi}^\dagger \boldsymbol{W}_j^{p,m} \boldsymbol{\Phi}\boldsymbol{c}_j, \quad \forall j \in \mathcal{J}.
\tag{43}
$$

All Loewner matrix blocks (33) are thus redefined as

$$
\mathbb{L}_{ij}^{p,m} = \frac{1}{\mu_i - \lambda_j} \left[\boldsymbol{V}_i^{p,m} - \boldsymbol{\Phi}\boldsymbol{\Phi}^\dagger \boldsymbol{W}_j^{p,m} \right] \boldsymbol{\Phi} \in \mathbb{C}^{\bar{q} \times \bar{k}}.
\tag{44}
$$

as well as the Loewner matrix (32) constructed from these blocks, which we denote as $\mathbb{L}_{pm}$. Constraining now the denominator to be shared among all $\bar{p} \times \bar{m}$ transfer matrix elements leads to the following coupled Loewner matrix problems

$$
\mathbb{L}_{pm}\boldsymbol{c} \approx \boldsymbol{0}_{\bar{\imath}\bar{q} \times 1}, \quad 1 \le p \le \bar{p}, \quad 1 \le m \le \bar{m}.
\tag{45}
$$

This, in turn, is equivalent to stacking all matrices $\mathbb{L}_{pm}$ as block-rows with any preferred ordering:

$$
\mathsf{L} = \begin{pmatrix} \mathbb{L}_{1,1} \\ \vdots \\ \mathbb{L}_{pm} \\ \vdots \\ \mathbb{L}_{\bar{p}\bar{m}} \end{pmatrix} \in \mathbb{C}^{\bar{\imath}\bar{q}\bar{p}\bar{m} \times \bar{\jmath}\bar{k}}.
\tag{46}
$$

The denominator coefficients are then found by solving

$$
\mathsf{L}\,\boldsymbol{c} \approx \boldsymbol{0}_{\bar{\imath}\bar{q}\bar{p}\bar{m} \times 1}.
\tag{47}
$$

If model realness is desired, then the real-valued blocks $\widehat{\mathbb{L}}_{ij}^{p,m}$, as defined in Section III-D, should be used instead of the complex-valued blocks $\mathbb{L}^{pm}$.

F. Handling a Large Number of Data Samples and/or Input/Output Ports

The MIMO case may lead to a large-size Loewner matrix L in case the number of input and output ports is large. The following discussion shows that L does not have to be assembled and stored at once, by exploiting a simple matrix compression strategy.

We start by casting (47) as a norm minimization problem, and we expand it in the equivalent form

$$
\min_{\boldsymbol{c}} \|\mathsf{L}\,\boldsymbol{c}\|_2^2 = \min_{\boldsymbol{c}} \left\{ \sum_{p,m} \|\mathbb{L}_{pm}\,\boldsymbol{c}\|_2^2 \right\}
\tag{48}
$$

In common situations, the Loewner matrix blocks $\mathbb{L}_{pm}$ are tall and thin matrices with significantly more rows than columns, since $\bar{\imath} \gg \bar{\jmath}$ and $\bar{q} \gg \bar{k}$, and thus $\bar{\imath}\bar{q} \gg \bar{\jmath}\bar{k}$. This suggests computing an "economy size" QR factorization of each block

$$
\mathbb{L}_{pm} = \mathsf{Q}_{pm}\mathsf{R}_{pm},
\tag{49}
$$

where the columns of $\mathsf{Q}_{pm} \in \mathbb{C}^{\bar{\imath}\bar{q} \times \bar{\jmath}\bar{k}}$ are orthogonal, $\mathsf{Q}_{pm}^H \mathsf{Q}_{pm} = \mathsf{I}$, and $\mathsf{R}_{pm} \in \mathbb{C}^{\bar{\jmath}\bar{k} \times \bar{\jmath}\bar{k}}$ is square and upper-triangular. Then,

$$
\|\mathbb{L}_{pm}\,\boldsymbol{c}\|_2^2 = \boldsymbol{c}^H \mathbb{L}_{pm}^H \mathbb{L}_{pm}\,\boldsymbol{c} = \boldsymbol{c}^H \mathsf{R}_{pm}^H \mathsf{R}_{pm}\,\boldsymbol{c} = \|\mathsf{R}_{pm}\,\boldsymbol{c}\|_2^2.
\tag{50}
$$

Therefore, we conclude that an equivalent formulation to (48) is provided by

$$
\min_{\boldsymbol{c}} \|\mathsf{R}\,\boldsymbol{c}\|_2^2
\tag{51}
$$

where

$$\mathbf{R} = \begin{pmatrix} \mathsf{R}_{1,1} \\ \vdots \\ \mathsf{R}_{pm} \\ \vdots \\ \mathsf{R}_{\bar{p}\bar{m}} \end{pmatrix} \in \mathbb{C}^{\bar{j}\bar{k}\bar{p}\bar{m} \times \bar{j}\bar{k}}, \qquad (52)$$

in which however the row size of $\mathbf{R}$ is much smaller than the row size of $\mathbf{L}$. Matrix $\mathbf{R}$ can be assembled directly from the $\mathbb{L}_{pm}$ blocks, without forming the entire matrix $\mathbf{L}$, thus leading to a large gain in memory occupation. The above compression is seamlessly applied to the real-valued formulation of Section III-D without modifications.

We remark that the above $\bar{p}\bar{m}$ individual QR factorizations (49) are independent and can be performed by processing separately the data samples of each transfer matrix element, possibly by splitting the workload into parallel threads running on a multicore processor. Note that the above-described QR processing is similar to the FastVF algorithm described in [45], [46], and later adapted to the Fast Parameterized Sanathanan-Koerner (FastPSK) iteration for data-driven multivariate parameterized macromodeling [21]. We therefore see that the proposed LM framework can inherit the good scalability properties from already well-established macromodeling schemes.

A further possible improvement stems from the fact that the Q_{pm} matrices in (49) are not needed, which allows the use of Q-less QR factorizations, providing a significant speed-up with respect to the standard QR decomposition. We make use of Q-less QR factorizations throughout our computational runs.

G. Summary

In summary, the proposed algorithm proceeds through the following steps (obvious modifications apply if the real-valued formulation is adopted):

1) split the frequency data in first and second partition. The size $\bar{j}$ of the first partition defines the number of poles in the rational barycentric form (12) of the model;
2) construct the matrices $\mathbb{L}_{ij}^{p,m}$ in (44);
3) perform the QR factorizations in (49);
4) assemble the blocks R_{pm} in $\mathbf{R}$ as in (52);
5) find the null space of $\mathbf{R}$, which provides the optimal set of denominator coefficients c_{jk};
6) reconstruct the numerator coefficients $d_j^{p,m}$ using (43).

As in the standard (non-parameterized) Loewner method, exact interpolation will not hold unless

- the underlying data samples come from the true evaluation of a rational function of frequency with polynomial coefficients, and
- the number of poles and the degree of the parameter-dependent polynomials at the numerator and denominator of the model match those of the original system.

Since the above conditions are generally not true, we seek for the vector that minimizes the residual $\|\mathbf{L}\,\boldsymbol{c}\|_2^2$ or, equivalently, $\|\mathbf{R}\,\boldsymbol{c}\|_2^2$. The closed-form solution to this problem is provided by the (right) singular vector $\boldsymbol{c}$ of $\mathbf{R}$ associated to the least singular value $\sigma_{\min}(\mathbf{R})$. Alternatively, the singular vector $\boldsymbol{c}_\star$

associated to any singular value $\sigma_* < \varepsilon$ can be used, where ε is a suitable threshold. The actual value of $\sigma_\star$ can be used to assess the quality of the overall model approximation both in frequency and parameter ranges. In practice, we prefer an a-posteriori metric to qualify the model, by computing the overall RMS model error $\mathcal{E}_{RMS}$, defined as

$$\mathcal{E}_{RMS}^2 = \frac{1}{\bar{l}\bar{q}\bar{p}\bar{m}} \sum_{l,q,p,m=1}^{\bar{l}\bar{q}\bar{p}\bar{m}} |\widehat{H}_{pm}(s_l,\theta_q) - H_{pm}(s_l,\theta_q)|^2. \quad (53)$$

The correlation between $\mathcal{E}_{RMS}$ and the selected singular value $\sigma_\star$ will be illustrated through the numerical examples in Section IV.

H. Order Selection

The above discussion assumes that the dynamical order $\bar{j}$ and the polynomial order $\bar{k}$ are given. These two parameters are however unknown in first place and should be estimated during the modeling process. Some algorithms exist [39], [40] that, in the standard (non-parameterized) Loewner framework, suggest a procedure that iteratively increase an initial order $\bar{j}_{\min}$ until a given approximation quality is attained.

Here, we adopt a similar iterative greedy strategy. We set the orders $\bar{j} = \bar{j}_{\min}$ and $\bar{k} = \bar{k}_{\min}$ to some initial (small) values, expecting that the resulting approximation error will be poor. At each iteration, we construct the models based on the order pairs $(\bar{j}, \bar{k})$ for all permutations of order values in the ranges $\bar{j} \in [\bar{j}_{\min}, \bar{j}_{\min} + 2]$ and $\bar{k} \in [\bar{k}_{\min}, \bar{k}_{\min} + 2]$. The resulting model characterized by the best approximation error is retained and used as a starting point for the next iteration. Iterations are stopped when the overall RMS approximation error is below a prescribed threshold.

I. Extension to Higher-Dimensional Parameter Spaces

All above derivations assumed that the parameter θ is a scalar. This is however not a limitation, since the same formulation is valid also for higher-dimensional parameter spaces with basically no modifications, as discussed below.

Assume that $\boldsymbol{\theta}$ is a vector with individual components θ^ν for $\nu = 1, \ldots, \bar{\nu}$. Each component requires its own grid of measurement points and its own polynomial basis. The resulting initial dataset becomes a high-dimensional $(\bar{\nu} + 1)$-way tensor (the extra dimension is for frequency), and the set of polynomial basis functions generalizes to a multivariate polynomial basis defined in a $\bar{\nu}$-dimensional hyper-rectangle. If this multivariate basis is defined through the Cartesian product of univariate bases $\{\varphi_{k_\nu}^\nu(\theta^\nu)\}$, one for each individual component θ^ν, then also the multivariate polynomial bases inherit a ν-way tensor structure. Such tensors are naturally described through multi-index vectors, $\boldsymbol{k} = (k_1, \ldots, k_{\bar{\nu}})$ for the basis and $\boldsymbol{q} = (q_1, \ldots, q_{\bar{\nu}})$ for the data points.

A much simpler equivalent approach is to number all measurement points in the parameter space and all individual multivariate basis functions using single (scalar) global linear indices, based on a suitable element ordering of the tensors. If we keep the same index symbols k, q that we used for the scalar case, then all derivations of this Section III apply

without modification. The upper bounds for those global linear indices can be related to the corresponding multi-indices through

$$\bar{k} = \prod_{\nu=1}^{\bar{\nu}} \bar{k}_\nu, \quad \bar{q} = \prod_{\nu=1}^{\bar{\nu}} \bar{q}_\nu. \quad (54)$$

J. Stability, Passivity, and Current Limitations

The proposed method extends to the (possibly multivariate) parameterized case the well-known Loewner framework, in an alternative way with respect to [43]. As such, the main limitations of the Loewner method are inherited by our scheme, including stability and passivity characterization and enforcement.

The stability of the system represented by the parametric rational function defined by (17) can be verified by checking the zeros of the denominator with respect to the frequency variable s, i.e., the zeros of the rational function

$$\sum_{j=1}^{\bar{j}} \frac{\sum_{k=1}^{\bar{k}} c_{jk}\varphi_k(\theta)}{s - \lambda_j}, \quad (55)$$

throughout and uniformly in the parameter domain Θ. This check can be performed only after the above model denominator is available through its coefficients c_{jk}. A discrete check at finite points $\hat{\theta}_q$ is straightforward by computing the denominator zeros for fixed $\theta = \hat{\theta}_q$, but

- there is no guarantee that any unstable zeros for other values of θ are not missed, since only a finite number of points can be checked, and
- more importantly, there is no way to enforce stability once unstable poles are detected.

Similar considerations apply for (uniform) passivity, which would require checking and enforcing that the transfer function of model (17) is positive or bounded real $\forall \theta \in \Theta$. For all documented examples, stability is checked over a fine parameter sweep after model construction. Results are discussed in Section IV.

Some stability-preserving and/or enforcing methods for multivariate macromodels are available, see e.g. [12], [13], [22], [23], [47]. Work is in progress to embed stability constraints similar to [23], so that at least all macromodel poles are guaranteed to have a negative real part $\forall \theta \in \Theta$. This work is not mature yet and will be documented in a future report. Conversely, passivity enforcement of a guaranteed stable model is indeed possible by exploiting the multivariate Hamiltonian characterization presented in [25], [26].

Another important limitation of the presented method comes from the inevitable curse of dimensionality that occurs when increasing the number of free variables. In particular, it is seen from (54) that the number of model coefficients and data points required for their evaluation, and hence memory and CPU cost, scale exponentially with the number of parameters $\bar{\nu}$. Therefore, as most closed-form data-driven parameterized model order reduction methods that are available in the literature, our method is limited to a small number of free parameters. In this work, we document examples with up to 2 free parameters.

IV. EXAMPLES

In this section, the proposed parameterized LM framework is applied to several test cases. Without loss of generality, Legendre polynomials are used as basis functions φ_k to capture the parametric dependence.

A. Chebyshev Filter

The first example considers a seventh-order Chebyshev low-pass filter, designed to have nominal cut-off frequency $f_0 = 2$ GHz, passband ripple $\varepsilon = 0.5$ dB, and impedance $Z_0 = 50$ Ω. The ideal component values for an optimal design are $C_1 = C_4 = 2.765$ pF, $L_1 = L_3 = 5.006$ nH, $C_2 = C_4 = 4.199$ pF, $L_2 = 5.349$ nH. However, the following component values, available from the market, are considered: $C_{1,4} = 2.7$ pF, $C_{2,4} = 4.3$ pF, $L_2 = 5.8$ nH. In addition, a parasitic dc resistance of 0.12 Ω is included in the inductor models. The parametric variable θ is here the cut-off frequency, which is swept in the range $\Theta = [1.5, 2.5]$ GHz. This corresponds to rescaling each component value by a factor f_0/θ.
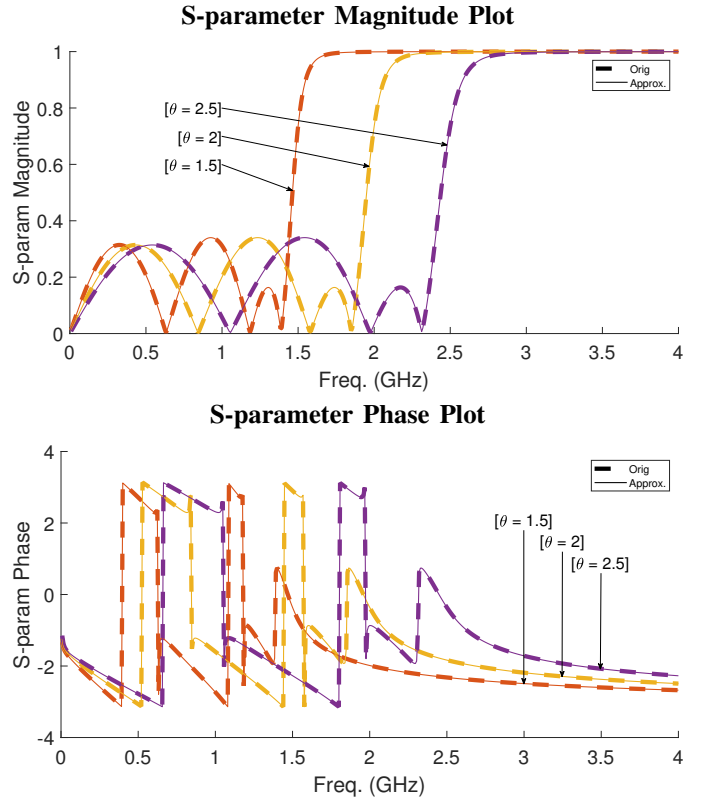

Fig. 1: Magnitude (top panel) and phase (bottom panel) of S_{11} for the Chebyshev filter example of Section IV-A, computed for different parameter values. Original data (thick dashed lines) are compared against macromodel responses (thin solid lines).

The two-port S-parameters of the filter are computed for $\bar{q} = 101$ parameter values at $\bar{l} = 501$ frequency points from dc to 4 GHz (both uniformly spaced). All these samples are used to build a macromodel using the proposed black-box multivariate LM interpolation. The frequency samples are

further divided into the two partitions, $\bar{j} = 4$ in partition Λ, and the remaining $\bar{i} = 496$ samples in partition $\mathcal{M}$. Based on the real-valued formulation, this corresponds to a model order of 7, matching the one of the actual system. Finally, $\bar{k} = 6$ polynomials (thus, up to order five) are used to approximate the parameter variation.
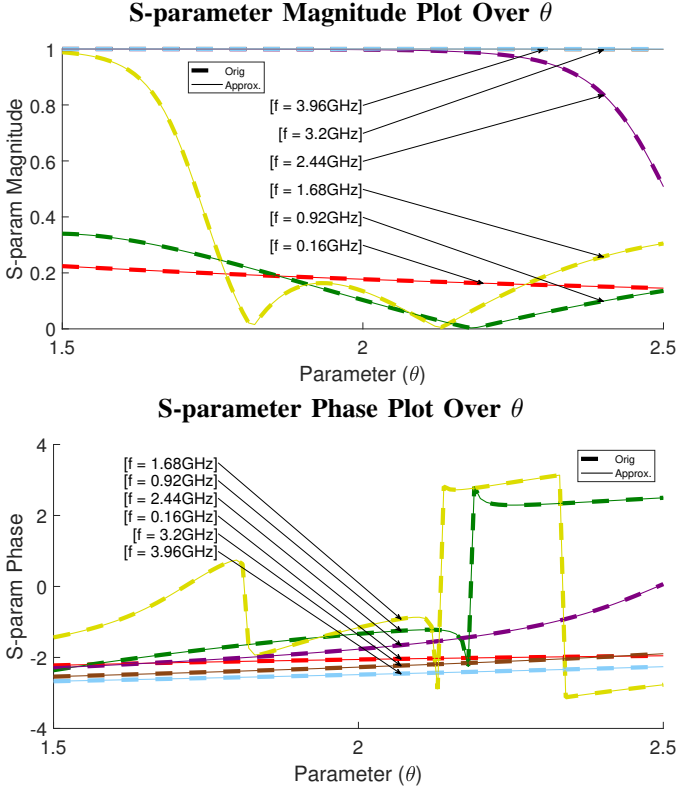

S-parameter Magnitude Plot Over θ

S-parameter Phase Plot Over θ

Fig. 2: Magnitude (top panel) and phase (bottom panel) of S_{11} for the Chebyshev filter example of Section IV-A, computed for different frequency values as a function of the parameter. Original data (thick dashed lines) are compared against macromodel responses (thin solid lines).

Approximation Error Magnitude Plot
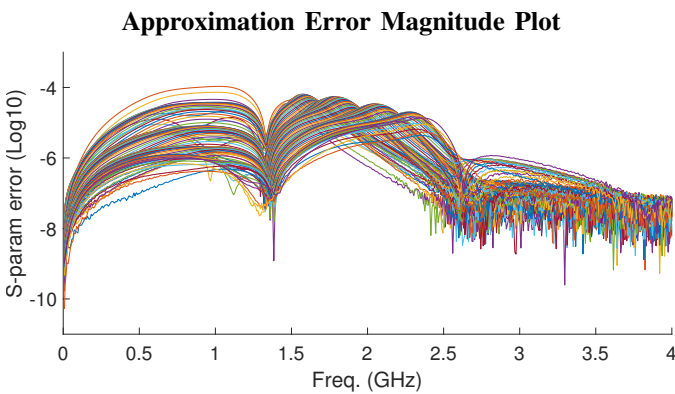
Fig. 3: Magnitude of the error on S_{11} between macromodel and original data for all the available parameter samples of the Chebyshev filter example.

Figure 1 shows the magnitude and phase of S_{11} over frequency for the minimum, central, and maximum value of the parameter. Figure 2 shows the variation of S_{11} with respect

to parameter θ at various frequency points. In both cases, the original data are compared against the macromodel, highlighting excellent accuracy The accuracy is further demonstrated by the errors on S_{11} for each of the 101 available parameter samples, provided in Figure 3. The maximum absolute error is below 10^{-4}.

Error vs Singular Value
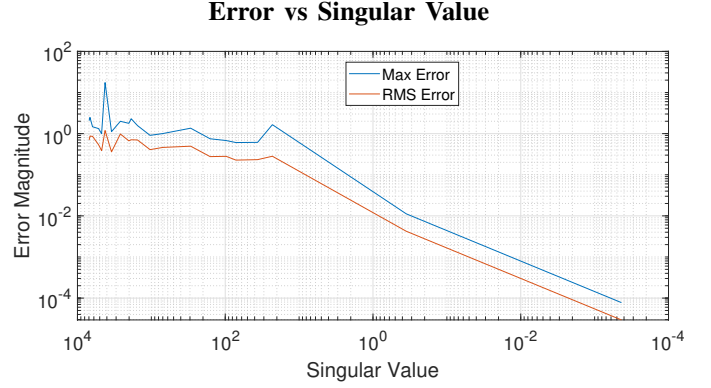
Fig. 4: Maximum and RMS approximation error against the singular value $\sigma_\star$ used to determine the model coefficients through the corresponding singular vector.

Figure 4 depicts the error in S_{11} at $\theta = 1.52$ as a function of the singular value $\sigma_\star$ chosen to identify the model coefficients. Both the RMS error and the maximum error over 500 frequency points are shown. As expected, a smaller $\sigma_\star$ leads to a more accurate multivariate macromodel. This figure shows that the choice of model coefficients is in fact not unique given a desired model accuracy level. The model turns outs to be uniformly stable over the entire parameter range. This was verified by a fine parameter sweep, as discussed in Section III-J.

B. Microstrip over Slotted Ground Plane

This example considers a microstrip (trace width $w = 0.035$ mm) running from end to end over a slotted ground plane (size: 10 cm $\times$ 10 cm, substrate with relative permittivity $\varepsilon_r = 4.7$ and thickness $t = 0.3$ mm). The slit (total length: 20 mm, width: 0.12 mm) is orthogonal to the microstrip with equal sidelength to the left and right of the microstrip longitudinal axis. The free parameter that we consider is the slit offset from the center of the microstrip, which ranges in the interval $\Theta = [1, 15]$ mm. For a more complete description of this geometry, see [23].

The initial parameterized frequency responses are computed using a time-domain field solver combined with an FFT postprocessing, resulting in 1858 frequency samples of the 2×2 scattering matrix, linearly spaced over the frequency band $[0, 10]$ GHz. A total of $\bar{q} = 15$ sets of scattering responses are available, corresponding to 1-mm steps in Θ.

Figure 5 reports the evolution of the proposed greedy order estimation process, by depicting the RMS error minimization path leading to the final frequency and parameter orders $\bar{j} = 17$ and $\bar{k} = 7$, respectively. The figure shows that, as expected, the RMS error decreases both along frequency and parameter directions almost monotonically. Figure 6 compares
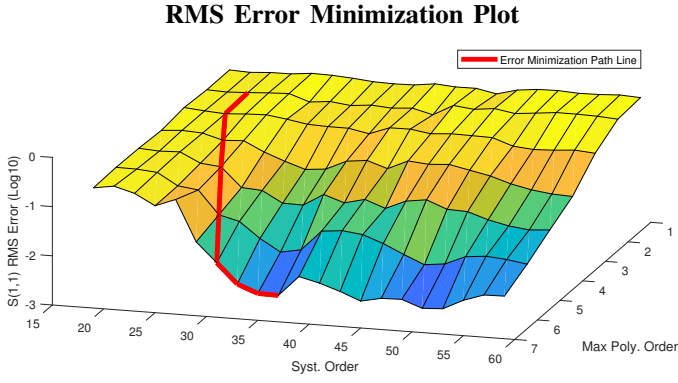
RMS Error Minimization Plot

Fig. 5: RMS error minimization path for the microstrip example of Section IV-B.

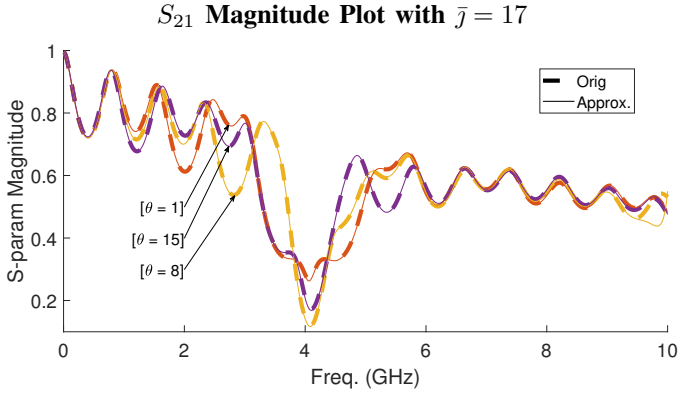S_{21} **Magnitude Plot with** $\bar{\jmath} = 17$

Fig. 6: Magnitude of S_{21} for the microstrip example of Section IV-B, computed for different parameter values. Original data (thick dashed lines) are compared against macromodel responses (thin solid lines).

the model responses to the original data for the magnitude of S_{21} and three parameter values, showing excellent agreement. The accuracy is confirmed by Figure 7, which provides the frequency-dependent model-vs-data error for all scattering matrix elements and for all parameter values. We see that this error has local minima at those frequencies that correspond to the frequency points in the first partition Λ. This behavior is expected and is a common feature of Loewner-based methods because of the exact interpolation conditions (13). The error however does not fall to zero exactly owing to our proposed polynomial approximation of these exact interpolation constraints.

The performance of the proposed scheme is compared in Figure 8 to the multivariate Loewner scheme of [43]. This figure reports the parameterized model response computed over a very fine sweep in the frequency and parameter plane, in order to check the smoothness of the interpolation/approximation at points that are not in the initial dataset, and for which we cannot therefore enforce accuracy. We see that our method (top panel) provides a uniformly smooth response, whereas the method of [43] (bottom panel) is affected by spurious oscillations and non-smooth behavior. This is readily explained by noting that [43] is based on a double rational barycentric approximation in both frequency and parameter,

Approximation Error Magnitude Plot with $\bar{\jmath} = 17$
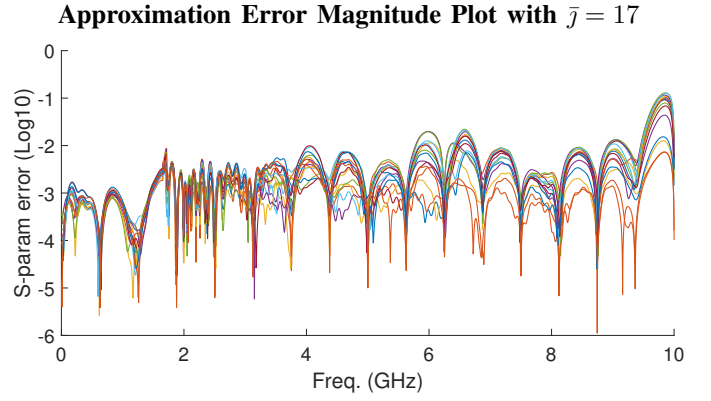

Fig. 7: Magnitude of model error over frequency, computed for all scattering matrix elements and available parameter samples for the microstrip example of Section IV-B.

which is enforced to interpolate exactly the initial responses at selected points in the frequency-parameter space. Nothing in that method prevents the occurrence of model poles in-between raw data samples, and this is exactly what appears from Figure 8. Conversely, our proposed method guarantees smoothness thanks to the overdetermined nature of the parameter fitting problem (26), whose least-squares formulation relaxes the exact interpolation constraints and results to be more robust.
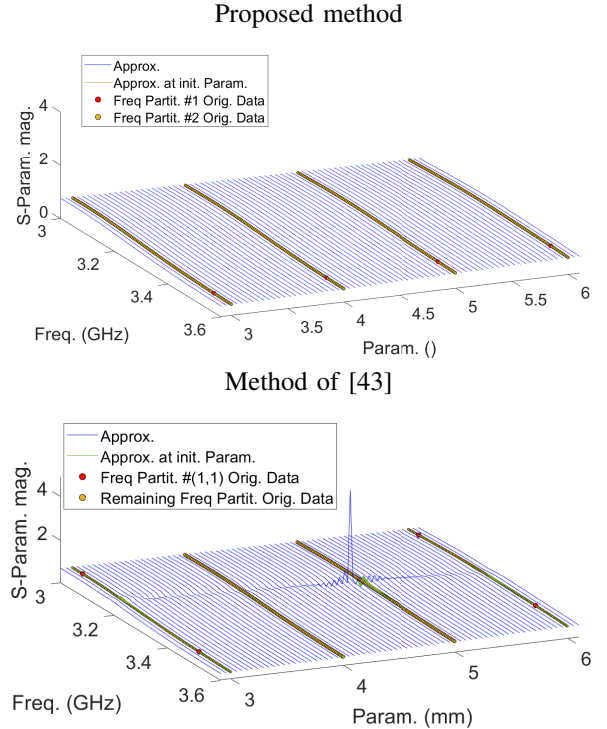
Proposed method

Method of [43]

Fig. 8: Magnitude of model response computed over a fine sweep in the frequency-parameter space (thin solid blue lines) with the proposed method (top panel) and the method of [43] (bottom panel).

Figure 9 depicts the trajectories of the model poles along the parameter space obtained by a fine parameter sweep, showing
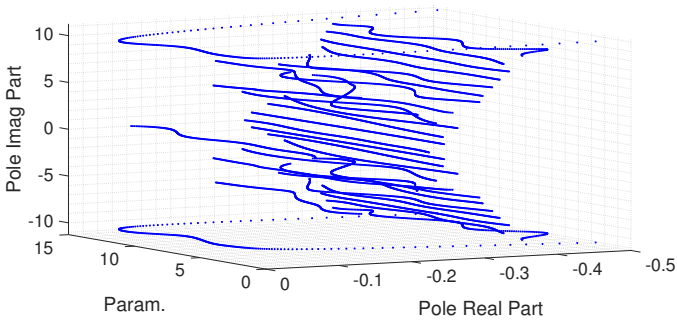
Poles Trajectories Over Parameter Range

Fig. 9: Poles trajectories along the parameter space for the microstrip example from Section IV-B.

continuous and smooth poles shifts as the parameter changes. Incidentally, the plot shows that the parametric system is stable throughout the parameter range, as none of the poles have real poles crossing the imaginary axis.

C. A High-Speed Multiboard Interconnect

This example refers to a high-speed interconnect routed through two multilayer PCBs [48] and one connector, with the inclusion of the corresponding via fields. The via diameter is fixed to 100 μm, whereas the antipad radius is a free parameter in the range $\Theta = [400, 600]$ μm. The number of ports of this structure is $\bar{m} = \bar{p} = 2$. A parameter sweep with $\bar{q} = 9$ sets of scattering responses, each with $\bar{l} = 500$ linearly distributed frequency samples spanning the band $[0, 10]$ GHz, were computed with a field solver and used for model extraction.

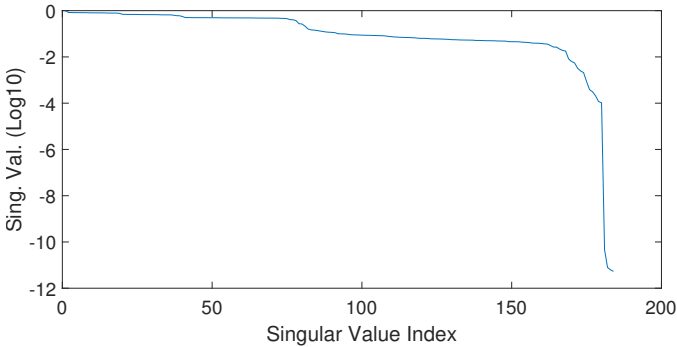**Loewner Matrix Singular Values**

Fig. 10: Normalized singular values of the parametric Loewner Matrix for the first example of Section IV-C (parametric variation of antipad radius).

The proposed algorithm led to $\bar{\jmath} = 23$ points in the first frequency partition Λ (resulting in a dynamical order of the resulting parameterized macromodel equal to 45) and $\bar{k} = 4$ polynomial basis functions, corresponding to a third-order polynomial approximation of the model coefficients.

The normalized singular value plot of the Loewner matrix is depicted in Figure 10, showing that the least (normalized) singular value is practically down to machine precision. The corresponding singular vector is thus a good approximation

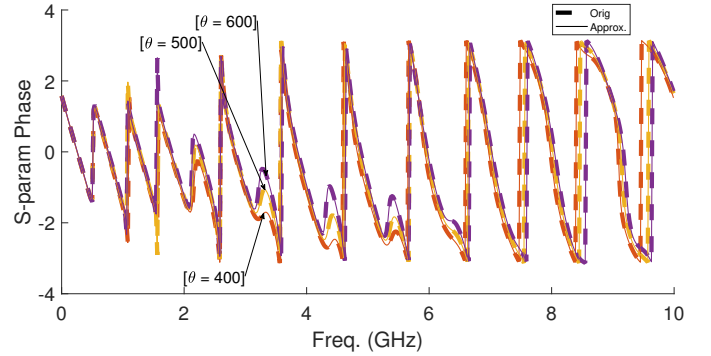**S-parameter Magnitude Plot**
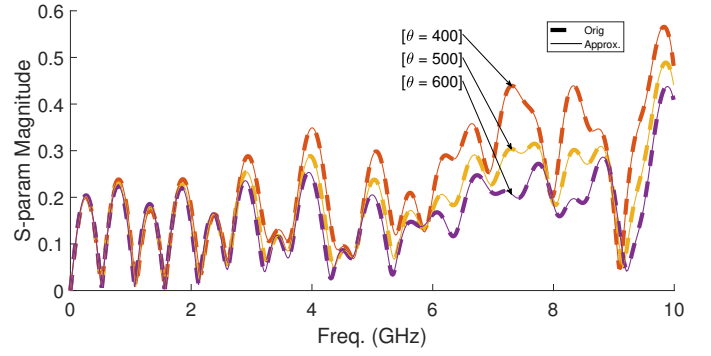
S-parameter Phase Plot

Fig. 11: Comparison between model and original data for the magnitude (top panel) and phase (bottom panel) of the scattering response S_{11} for the first example of Section IV-C (parametric variation of antipad radius).

of the LM null space and is used to define the model coefficients. Figure 11 compares the magnitude and phase of S_{11} obtained from the model versus original data, for three selected parameter values. These figures show an excellent agreement between model and data. The accuracy is further confirmed by Figure 12a, reporting the absolute (RMS) model error for all available parameter data samples. We see that the error is uniformly below 10^{-3}, except for the upper frequencies. A better control of local model accuracy can be obtained by a dedicated selection of points in the first partition Λ. For instance, Figure 12b shows that increasing the density of the first partition points at high frequencies significantly improves accuracy with respect to a uniform sampling (cfr. top panel). Note that for this example, after checking for stability, we determined that the macromodel is stable over the entire parameter range.

For this example, a parameterized model was also generated by applying the PSK scheme of [23]. The resulting errors on all responses are depicted in Figure 12c. Since the latter method is based on an iterative least squares process, without explicit exact interpolation constraints as in the proposed Loewner approach, the error is more uniformly distributed along frequency, without well-defined "deeps". In any case, both methods provide parameterized models of excellent accuracy.

We now consider the same structure, but with a different parameter. Namely, the via radius spanning the range $\Theta =$

(a) Approximation Error (Loewner, uniform)

(b) Approximation Error (Loewner, nonuniform)
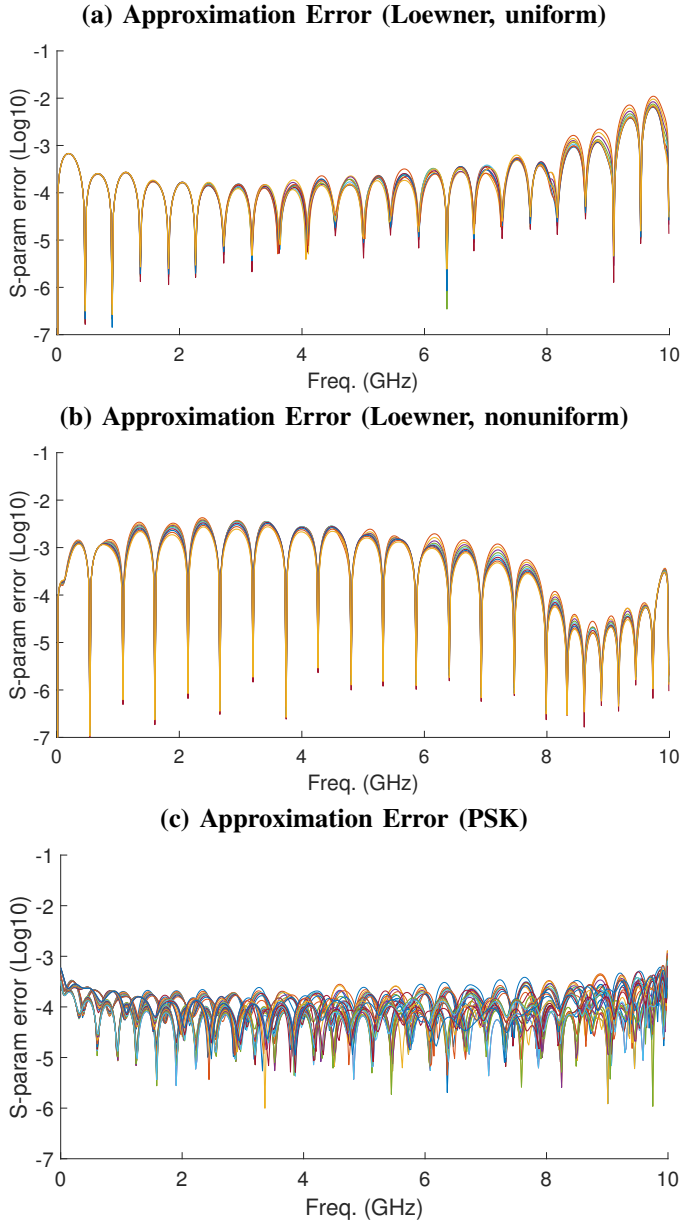

(c) Approximation Error (PSK)

Fig. 12: Magnitude of model error over frequency, computed for all scattering matrix elements and available parameter samples for the first example of Section IV-C (parametric variation of antipad radius): (a) proposed Loewner approach with uniformly distributed points in the first partition Λ; (b) proposed Loewner approach with a denser distribution of first partition points at high frequencies; (c) PSK algorithm of [23].

$[100, \ 300]$ μm, with a fixed antipad radius of 400 μm. All parameters and model orders are the same as above. Figure 13 and 14 report the model vs data comparison for three selected parameter values and the cumulative RMS model error plot, respectively, from which we can confirm the good accuracy of the proposed parametrized interpolation/approximation. After performing a fine parameter sweep, it was found that the marcomodel is stable over 72% of the initial parameter range. This highlights the issue of non-guaranteed stability mentioned in Section III-J. However, if we reduced $\bar{\jmath} = 23$ to $\bar{\jmath} = 22$, we

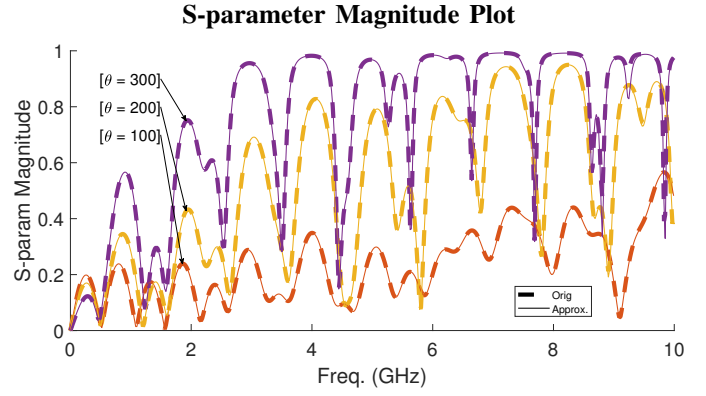### S-parameter Magnitude Plot

Fig. 13: Comparison between model and original data for the magnitude of the scattering response S_{11} for the second example of Section IV-A (parametric variation of via radius).

could achieve 100% stability over the parameter range for a small loss in accuracy.
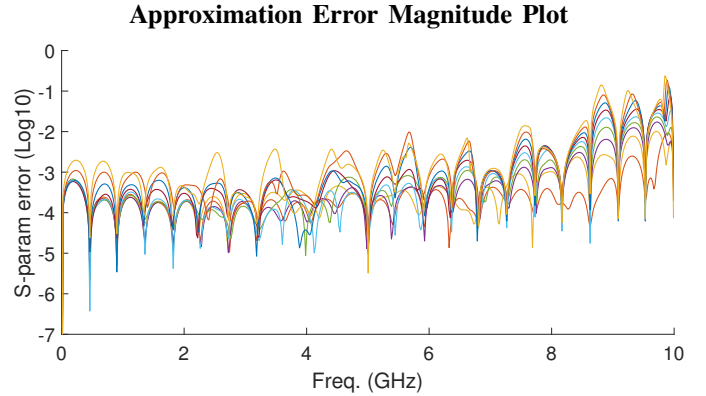
Approximation Error Magnitude Plot

Fig. 14: Magnitude of model error over frequency, computed for all scattering matrix elements and available parameter samples for the second example of Section IV-A (parametric variation of via radius).

D. Node-to-Node Bus

We now turn to a multivariate case with $\nu = 2$ free parameters. The case study regards the node-to-node bus described in [49], in which however the length of the single microstrip lines $M_{1,2}$ and $S_{1,2,5,6,7}$ is reduced by half. The two free parameters are the gap of the coupled lines $C_{1,2}$, in the range $[40, 120]$ μm, and the length of line C_1, in the range $[80, 120]$ mm.

The structure was simulated for an evenly-spaced grid of 31×31 parameter samples at 501 frequency points from dc to 5 GHz. Of these frequency samples, $\bar{\jmath} = 50$ are used for partition Λ, and the remaining $\bar{\imath} = 450$ samples (with dc excluded) are used for partition $\mathcal{M}$. The model order is thus 99. As to the parametric dependence, polynomials up to order six and four are used to model parameters θ_1 and θ_2, respectively. The total number of bivariate polynomials is thus 35.

Figure 15 shows the real and imaginary part of the far-end crosstalk at the termination of the bottom via chip line,

TABLE I: Loewner matrix sizes and CPU time required by the SVD computation using the standard SVD and the proposed approach (QR+SVD), for the considered test cases.

	LM size	Standard SVD (s)	QR+SVD (s)
Ex. A	400768×48	0.621	0.264
Ex. B	220686×288	2.790	1.513
Ex. C	34333×184	0.204	0.097
Ex. D	1729800×3500	1557	1057
Ex. D$'$	259200×3500	237.4	162.6

denoted as "BLL$_{22}$" in [49]. Simulation results are compared against macromodel responses for various samples of the gap, with the line length constrained to a fixed value, and vice versa. The accuracy of the proposed macromodeling approach is confirmed also for this multivariate case. Figure 16 shows the maximum error over frequency between model and original data. The error is well below 0.01 except for the highest frequencies. Note that after checking for stability, this two-variate parametric system is found to be non-stable. This highlights the fact that stability is not guaranteed by construction as discussed in Section III-J. Addressing macromodel stability is an important future direction related to this work.

E. Efficiency

As discussed in Section III-F, the proposed approach has some inherent advantages with respect to standard Loewner-based methods for what concerns memory footprint and efficiency. In order to confirm this statement, we report in Table I the size of the Loewner matrices for the four examples discussed in this paper, together with the runtime required using both the suggested QR+SVD implementation and the direct approach (plain SVD). The last row, denoted as D$'$ in the table, repeats the two-parameter test case D by reducing the initial dataset. An economy-size SVD was used in all cases to save memory occupation. Therefore, despite the large size of the Loewner matrices in some cases, all examples could be processed also by means of the standard SVD approach. In all cases, the proposed QR+SVD approach was able to perform the same computations in less time. Nevertheless, we remark that the most important advantage is the substantial reduction in memory occupation provided by operating on the (much) smaller matrix **R**.

V. CONCLUSIONS

In this paper, we proposed a parametric black-box macromodeling method based on Loewner interpolation. This new method embeds orthogonal polynomials as an integral part of the parameterization framework. We validated the method using several examples relevant for signal and power integrity applications. The examples illustrate the accuracy of the proposed method, and its ability to control model smoothness in the parameter space as compared to existing techniques in the Loewner framework.

VI. ACKNOWLEDGMENT

REFERENCES

[1] S. Grivet-Talocia and B. Gustavsen, *Passive Macromodeling: Theory and Applications*. New York: John Wiley and Sons, 2016.

[2] R. Achar and M. S. Nakhla, "Efficient transient simulation of embedded subnetworks characterized by s-parameters in the presence of nonlinear elements," *IEEE Transactions on Microwave Theory and Techniques*, vol. 46, no. 12, pp. 2356–2363, Dec 1998.

[3] C. P. Coelho, J. R. Phillips, and L. M. Silveira, "Passive constrained rational approximation algorithm using nevanlinna-pick interpolation," in *Proceedings 2002 Design, Automation and Test in Europe Conference and Exhibition*, March 2002, pp. 923–930.

[4] R. Achar, P. K. Gunupudi, M. Nakhla, and E. Chiprout, "Passive interconnect reduction algorithm for distributed/measured networks," *IEEE Transactions on Circuits and Systems II: Analog and Digital Signal Processing*, vol. 47, no. 4, pp. 287–301, April 2000.

[5] W. T. Beyene and J. E. Schutt-Aine, "Efficient transient simulation of high-speed interconnects characterized by sampled data," *IEEE Transactions on Components, Packaging, and Manufacturing Technology: Part B*, vol. 21, no. 1, pp. 105–114, Feb 1998.

[6] W. T. Beyene and J. Schutt-Aine, "Accurate frequency-domain modeling and efficient circuit simulation of high-speed packaging interconnects," *IEEE Transactions on Microwave Theory and Techniques*, vol. 45, no. 10, pp. 1941–1947, Oct 1997.

[7] M. Elzinga, K. L. Virga, L. Zhao, and J. L. Prince, "Pole-residue formulation for transient simulation of high-frequency interconnects using householder ls curve-fitting techniques," *IEEE Transactions on Advanced Packaging*, vol. 23, no. 2, pp. 142–147, May 2000.

[8] B. Gustavsen and A. Semlyen, "Rational approximation of frequency domain responses by vector fitting," *IEEE Transactions on Power Delivery*, vol. 14, no. 3, pp. 1052–1061, 1999.

[9] M. Elzinga, K. L. Virga, and J. L. Prince, "Improved global rational approximation macromodeling algorithm for networks characterized by frequency-sampled data," *IEEE Transactions on Microwave Theory and Techniques*, vol. 48, no. 9, pp. 1461–1468, Sep. 2000.

[10] S.-H. Min and M. Swaminathan, "Efficient construction of two-port passive macromodels for resonant networks," in *IEEE 10th Topical Meeting on Electrical Performance of Electronic Packaging (Cat. No. 01TH8565)*, Oct 2001, pp. 229–232.

[11] F. Ferranti, T. Dhaene, and L. Knockaert, "Compact and passive parametric macromodeling using reference macromodels and positive interpolation operators," *IEEE Transactions on Components, Packaging and Manufacturing Technology*, vol. 2, no. 12, pp. 2080–2088, 2012.

[12] F. Ferranti, L. Knockaert, and T. Dhaene, "Passivity-preserving parametric macromodeling by means of scaled and shifted state-space systems," *IEEE Transactions on Microwave Theory and Techniques*, vol. 59, no. 10, pp. 2394–2403, 2011.

[13] F. Ferranti, L. Knockaert, T. Dhaene, and G. Antonini, "Passivity-preserving parametric macromodeling for highly dynamic tabulated data based on lur'e equations," *IEEE Transactions on Microwave Theory and Techniques*, vol. 58, no. 12, pp. 3688–3696, 2010.

[14] F. Ferranti, L. Knockaert, and T. Dhaene, "Guaranteed passive parameterized admittance-based macromodeling," *IEEE Transactions on Advanced Packaging*, vol. 33, no. 3, pp. 623–629, 2010.

[15] D. Deschrijver and T. Dhaene, "Stability and passivity enforcement of parametric macromodels in time and frequency domain," *IEEE Transactions on Microwave Theory and Techniques*, vol. 56, no. 11, pp. 2435–2441, 2008.

[16] T. Dhaene and D. Deschrijver, "Stable parametric macromodeling using a recursive implementation of the vector fitting algorithm," *IEEE Microwave and Wireless Components Letters*, vol. 19, no. 2, pp. 59–61, 2009.

[17] P. Triverio, S. Grivet-Talocia, and M. S. Nakhla, "A parameterized macromodeling strategy with uniform stability test," *IEEE Transactions on Advanced Packaging*, vol. 32, no. 1, pp. 205–215, 2009.

[18] D. Deschrijver, T. Dhaene, and D. D. Zutter, "Robust parametric macromodeling using multivariate orthonormal vector fitting," *IEEE Transactions on Microwave Theory and Techniques*, vol. 56, no. 7, pp. 1661–1667, 2008.

[19] P. Triverio, M. S. Nakhla, and S. Grivet-Talocia, "Passive parametric macromodeling from sampled frequency data," in *2010 IEEE 14th Workshop on Signal Propagation on Interconnects*, 2010, pp. 117–120.
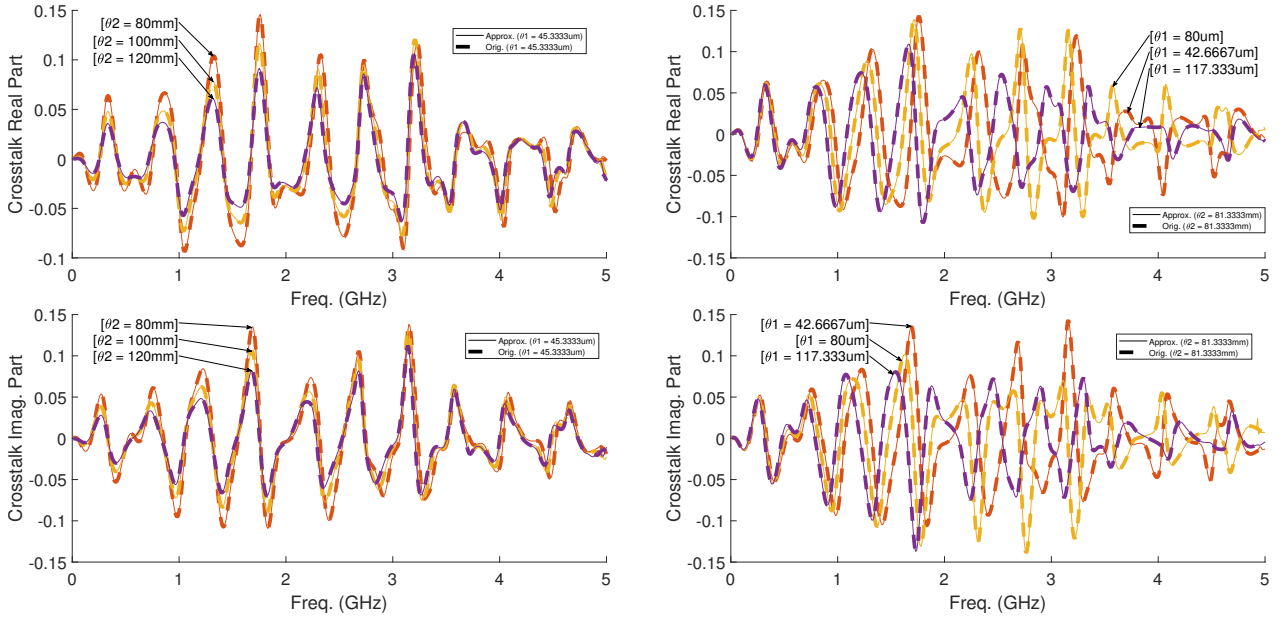
Fig. 15: Far-end crosstalk in the node-to-node bus of Section IV-D. Left panels: real (top) and imaginary part (bottom) of crosstalk for different values of θ_2 and fixed $\theta_1 = 45.3333$ μm; right panels: real (top) and imaginary part (bottom) of crosstalk for different values of θ_1 and fixed $\theta_2 = 81.3333$ mm.
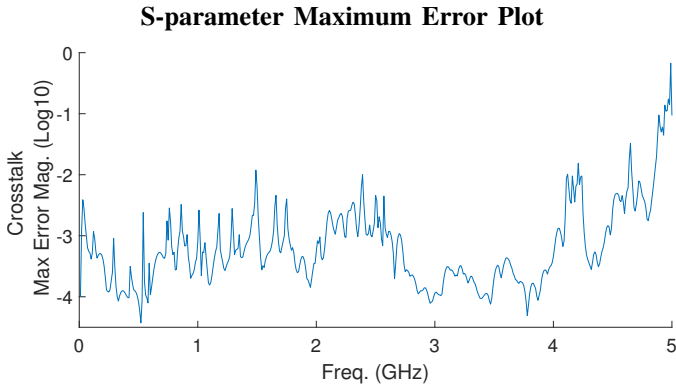

Fig. 16: Maximum error over frequency for the node-to-node bus example of Section IV-D.

[20] P. Triverio, M. Nakhla, and S. Grivet-Talocia, "Passive parametric modeling of interconnects and packaging components from sampled impedance, admittance or scattering data," in *3rd Electronics System Integration Technology Conference ESTC*, 2010, pp. 1–6.

[21] T. Bradde, S. Grivet-Talocia, M. D. Stefano, and A. Zanco, "A scalable reduced-order modeling algorithm for the construction of parameterized interconnect macromodels from scattering responses," in *2018 IEEE Symposium on Electromagnetic Compatibility, Signal Integrity and Power Integrity (EMC, SI PI)*, July 2018, pp. 650–655.

[22] E. R. Samuel, L. Knockaert, F. Ferranti, and T. Dhaene, "Guaranteed passive parameterized macromodeling by using sylvester state-space realizations," *IEEE Transactions on Microwave Theory and Techniques*, vol. 61, no. 4, pp. 1444–1454, April 2013.

[23] S. Grivet-Talocia and R. Trinchero, "Behavioral, parameterized, and broadband modeling of wired interconnects with internal discontinuities," *IEEE Transactions on Electromagnetic Compatibility*, vol. 60, no. 1, pp. 77–85, Feb 2018.

[24] S. Grivet-Talocia and E. Fevola, "Compact parameterized black-box modeling via fourier-rational approximations," *IEEE Transactions on Electromagnetic Compatibility*, vol. 59, no. 4, pp. 1133–1142, Aug 2017.

[25] S. Grivet-Talocia, "A perturbation scheme for passivity verification and enforcement of parameterized macromodels," *IEEE Transactions on Components, Packaging and Manufacturing Technology*, vol. 7, no. 11, pp. 1869–1881, Nov 2017.

[26] A. Zanco, S. Grivet-Talocia, T. Bradde, and M. De Stefano, "Enforcing passivity of parameterized lti macromodels via hamiltonian-driven multivariate adaptive sampling," *IEEE Transactions on Computer-Aided Design of Integrated Circuits and Systems*, vol. PP, pp. 1–1, 11 2018.

[27] A. C. Antoulas and B. D. Q. Anderson, "On the scalar rational interpolation problem," *IMA Journal of Mathematical Control and Information*, vol. 3, no. 2-3, pp. 61–88, 1986.

[28] B. D. O. Anderson and A. C. Antoulas, "Rational interpolation and state-variable realizations," *Linear Algebra and its Applications*, vol. 137-138, pp. 479 – 509, 1990. [Online]. Available: http://www.sciencedirect.com/science/article/pii/0024379590901408

[29] A. C. Antoulas and B. D. O. Anderson, *State-space and Polynomial approaches to Rational Interpolation*, K. M. A., van Schuppen J. H., and R. A. C. M., Eds. Boston, MA: Birkhäuser Boston, 1990.

[30] A. Mayo and A. Antoulas, "A framework for the solution of the generalized realization problem," *Linear Algebra and its Applications*, vol. 425, no. 2, pp. 634 – 662, 2007, special Issue in honor of Paul Fuhrmann. [Online]. Available: http://www.sciencedirect.com/science/article/pii/S0024379507001280

[31] S. Lefteriu and A. C. Antoulas, "Modeling multi-port systems from frequency response data via tangential interpolation," in *2009 IEEE Workshop on Signal Propagation on Interconnects*, May 2009, pp. 1–4.

[32] M. T. Kassis, M. Kabir, Y. Q. Xiao, and R. Khazaka, "Passive reduced order macromodeling based on loewner matrix interpolation," *IEEE Transactions on Microwave Theory and Techniques*, vol. 64, no. 8, pp. 2423–2432, Aug 2016.

[33] M. Kabir and R. Khazaka, "Macromodeling of distributed networks from frequency-domain data using the loewner matrix approach," *IEEE Transactions on Microwave Theory and Techniques*, vol. 60, no. 12, pp. 3927–3938, Dec 2012.

[34] ——, "Loewner matrix macromodeling for y-parameter data with a priori **D** matrix extraction," *IEEE Transactions on Microwave Theory and Techniques*, vol. 64, no. 12, pp. 4098–4107, Dec 2016.

[35] Y. Wang, C. Lei, G. K. H. Pang, and N. Wong, "Mfti: Matrix-format tangential interpolation for modeling multi-port systems," in *Design Automation Conference*, June 2010, pp. 683–686.

[36] M. Sahouli and A. Dounavis, "Delay extraction-based modeling using loewner matrix framework," *IEEE Transactions on Components, Packaging and Manufacturing Technology*, vol. 7, no. 3, pp. 424–433, March 2017.

[37] M. Sahouli, S. Wahid, and A. Dounavis, "Iterative loewner matrix macromodeling approach for noisy frequency responses," *IEEE Transac-

tions on Microwave Theory and Techniques, vol. 67, no. 2, pp. 634–641, Feb 2019.

[38] M. Kabir, Y. Q. Xiao, and R. Khazaka, "Loewner matrix interpolation for noisy s-parameter data," in *2016 IEEE 25th Conference on Electrical Performance Of Electronic Packaging And Systems (EPEPS)*, Oct 2016, pp. 95–98.

[39] Y. Nakatsukasa, O. Ste, and L. N. Trefethen, "The aaa algorithm for rational approximation," *SIAM Journal on Scientific Computing*, vol. 40, no. 3, p. A1494A1522, 2018.

[40] A. Hochman, "Fastaaa: A fast rational-function fitter," in *2017 IEEE 26th Conference on Electrical Performance of Electronic Packaging and Systems (EPEPS)*, Oct 2017, pp. 1–3.

[41] M. Kabir and R. Khazaka, "Parametric macromodeling of high-speed modules from frequency-domain data using loewner matrix based method," in *2013 IEEE MTT-S International Microwave Symposium Digest (MTT)*, June 2013, pp. 1–4.

[42] M. Kabir and R. Khazaka, "Fixed-order parametric macromodeling of interconnects from s-parameter data using loewner matrix based method," in *2013 IEEE 22nd Conference on Electrical Performance of Electronic Packaging and Systems*, Oct 2013, pp. 141–144.

[43] A. Ionita and A. Antoulas, "Data-driven parametrized model reduction in the loewner framework," *SIAM Journal on Scientific Computing*, vol. 36, no. 3, pp. A984–A1007, 2014.

[44] A. Antoulas, A. Ionita, and S. Lefteriu, "On two-variable rational interpolation," *Linear Algebra and its Applications*, vol. 436, no. 8, pp. 2889 – 2915, 2012.

[45] D. Deschrijver, M. Mrozowski, T. Dhaene, and D. D. Zutter, "Macro-modeling of multiport systems using a fast implementation of the vector fitting method," *IEEE Microwave and Wireless Components Letters*, vol. 18, no. 6, pp. 383–385, 2008.

[46] A. Chinea and S. Grivet-Talocia, "On the parallelization of vector fitting algorithms," *IEEE Transactions on Components, Packaging and Manufacturing Technology*, vol. 1, no. 11, pp. 1761–1773, Nov 2011.

[47] F. Ferranti, L. Knockaert, and T. Dhaene, "Parameterized s-parameter based macromodeling with guaranteed passivity," *IEEE Microwave and Wireless Components Letters*, vol. 19, no. 10, pp. 608–610, 2009.

[48] J. Preibisch, T. Reuschel, K. Scharff, J. Balachandran, B. Sen, and C.Schuster, "Exploring efficient variability-aware analysis method forhigh-speed digital link design using pce," *DesignCon*, 2017.

[49] M. Larbi, I. S. Stievano, F. G. Canavero, and P. Besnier, "Variability impact of many design parameters: The case of a realistic electronic link," *IEEE Transactions on Electromagnetic Compatibility*, vol. 60, no. 1, pp. 34–41, Feb 2018.

Stefano Grivet-Talocia (M'98–SM'07–F'18) received the Laurea and Ph.D. degrees in electronic engineering from the Politecnico di Torino, Turin, Italy. From 1994 to 1996, he was with the NASA/Goddard Space Flight Center, Green- belt, MD, USA. He is currently a Full Professor of electrical engineering with the Politecnico di Torino. He co-founded the academic spinoff company IdemWorks in 2007, serving as the President until its acquisition by CST in 2016. He has authored over 150 journal and conference papers. His current research interests include passive macromodeling of lumped and distributed interconnect structures, model-order reduction, modeling and simulation of fields, circuits, and their interaction, wavelets, time-frequency transforms, and their applications.

Dr. Grivet-Talocia was a co-recipient of the 2007 Best Paper Award of the IEEE TRANSACTIONS ON ADVANCED PACKAGING. He received the IBM Shared University Research Award in 2007, 2008, and 2009. He was an Associate Editor of the IEEE TRANSACTIONS ON ELECTROMAGNETIC COMPATIBILITY from 1999 to 2001 and He is currently serving as Associate Editor for the IEEE TRANSACTIONS ON COMPONENTS, PACKAGING AND MANUFACTURING TECHNOLOGY. He was the General Chair of the 20th and 21st IEEE Workshops on Signal and Power Integrity (SPI2016 and SPI2017).
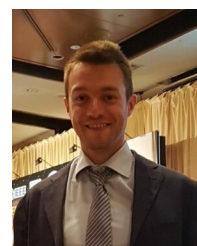
Paolo Manfredi (S'10–M'14–SM'18) received the M.Sc. degree in electronic engineering from the Politecnico di Torino, Torino, Italy, in 2009, and the Ph.D. degree in information and communication technology from the Scuola Interpolitecnica di Dottorato, Politecnico di Torino, in 2013.

From 2013 to 2014, he was a Postdoctoral Researcher with the EMC Group, Politecnico di Torino. From 2014 to 2017, he was a Postdoctoral Research Fellow of the Research Foundation–Flanders (FWO) with the Electromagnetics Group, Department of Information Technology, Ghent University, Ghent, Belgium. He is currently an Assistant Professor with the EMC Group, Department of Electronics and Telecommunications, Politecnico di Torino. His research interests comprise the several aspects of circuit and interconnect modeling and simulation, including statistical and worst-case analysis, signal integrity, and electromagnetic compatibility.

Prof. Manfredi was a recipient of an Outstanding Young Scientist Award at the 2018 Joint IEEE International Symposium on Electromagnetic Compatibility & Asia-Pacific Symposium on Electromagnetic Compatibility, the Best Paper Award at the 2016 IEEE Electrical Design of Advanced Packaging and Systems Symposium, the Best Oral Paper Award and the Best Student Paper Award at the 22nd and 19th IEEE Conference on Electrical Performance of Electronic Packaging and Systems, respectively, a Young Scientist Award at the XXX International Union of Radio Science General Assembly and Scientific Symposium, and an Honorable Mention at the 2011 IEEE Microwave Theory and Techniques Society International Microwave Symposium.

Yi Qing Xiao (GSM'15) received his bachelor and Master degrees in Electrical Engineering from McGill University, Montreal, Quebec, Canada in 2015 and 2017, respectively. He is currently completing his Ph.D. in Electrical Engineering in McGill University. His research interests include electronic design automation and simulation of integrated circuits and microsystems.

Mr. Xiao is a recipient of the Hydro-Quebec Masters in Engineering Award during his time pursuing his Master degree and the McGill Engineering Doctoral Award for his Ph.D. studies.

Roni Khazaka (S'92-M'03-SM'07) received his Bachelor, Master and PhD degrees in Electrical Engineering from Carleton University, Ottawa, Canada in 1995, 1998 and 2002 respectively. In 2002, he joined the department of electrical and computer engineering at Mcgill University, Montréal, Canada, where he currently is an associate professor. In 2009 he was a visiting research fellow at the university of Shizuoka, Japan. In, 2017 he was a visiting research at Politecnico di Torino, Torino, Italy. Prof. Khazaka has authored over 70 journal and conference papers on the simulation of high-speed interconnects and RF circuits, his current research interests include electronic design automation, numerical algorithms and techniques, and the analysis and simulation of RF ICs, and high-speed interconnects.

Prof. Khazaka's past awards and scholarships include the Microwave Theory and Techniques society's 2002 Microwave Prize, The Natural Sciences and Engineering Research Council (NSERC) of Canada scholarships (at the masters and doctoral levels), Carleton University's Senate Medal and University Medal in Engineering, the Nortel Networks scholarship and the IBM cooperative fellowship.

Prof. Khazaka served on several IEEE committees. He is the founding chair of the Montreal IEEE CEDA council chapter. He was IEEE Montreal section treasurer (2005/2006), and IEEE Montreal Section Chair (2013/2014). He is a member of the technical program committee of signal propagation on interconnects workshop since 2006, the technical program review committee of the International Microwave Symposium since 2012, and the technical program committee of EPEPS since 2016. He served on the organizing committee and numerous conferences such as ISCAS, MWCAS, NEWCAS, ISSSE, CCECE, and the International Microwave Symposium (IMS). He was co-chair and general chair of the IEEE Electrical Performance of Electronic Packaging and Systems conference in 2018 and 2019 respectively.